MODELING PORE GEOMETRIC AND WETTABILITY TRENDS OF MULTIPHASE FLOW IN POROUS MEDIA

P.H. Valvatne, X.D. Jing and R.M.M. Smits
Shell International E&P, Rijswijk, The Netherlands

This paper was prepared for presentation at the International Symposium of the Society of Core Analysts held in Abu Dhabi, UAE, 5-9 October, 2004

ABSTRACT

Using geologically realistic pore networks it is possible to predict relative permeability and imbibition capillary pressure using pore-scale modeling. Starting with a network representation of Berea sandstone the pore throat radii are adjusted to match mercury injection capillary pressure and pore volumes are adjusted to match the Nuclear Magnetic Resonance (NMR) response, while keeping the rank order of radii and volumes and the network topology. Then predictions of single and multiphase properties are made with no further adjustment of the model. Empirical correlations in terms of reservoir properties like permeability, porosity, rock type and wettability, are often used to estimate relative permeability in cases where experimental data are not available. However, due to the limited experimental data that have been obtained following modern SCAL measurement and interpretation procedures, it is difficult to assess whether the correlations are valid for the full range of possible reservoir conditions, especially with respect to wettability. In this paper we show how pore-scale network modeling can be used to investigate the range and limitations of empirical correlations by varying pore geometric and wettability properties commonly used in correlations.

INTRODUCTION

In network modeling the void space of a rock is represented at the microscopic scale by a lattice of pores connected by throats. By applying rules that govern the transport and distribution of fluids in pores and throats, macroscopic properties, for instance capillary pressure or relative permeability, can then be computed across the network, which typically consists of several thousand pores and throats representing a rock sample of a few millimeters cubed. Until recently most networks were based on a regular topology that does not reflect the random nature of real porous rock. For complex sandstones it is usually necessary to first create a 3D voxel based representation of the pore space that should capture the statistics of the real rock [1, 2]. From this voxel representation an equivalent network of pores and throats can be extracted [1, 3]. Individual elements are given properties (inscribed radius, volume etc.) recorded straight from the original voxel image. Using these realistic networks water-wet experimental data have been successfully predicted for Bentheimer [4] and Berea sandstones [5]. The approach as presented by Øren *et al.* assumes that lattice and subsequent flow predictions are specific to the properties of the porous medium used in the voxel-based reconstruction. Valvatne

and Blunt [6] proposed a methodology for combining realistic networks, originally constructed to represent one particular porous medium, with conditioning to experimental capillary pressure data to predict flow properties of a variety of different porous media. In this paper we will extend this methodology by including nuclear magnetic resonance (NMR) data.

NETWORK MODEL

We use a two-phase capillary dominated network model that broadly follows the work of Øren, Patzek and coworkers [4, 7]. Further details, including relevant equations, can be found elsewhere [4, 6-8]. The model simulates primary oil flooding, wettability alteration and any subsequent cycles of water and oil flooding. A three-dimensional voxel representation of Berea sandstone is the basis for the networks used in this paper [9], Figure 1. A topologically equivalent network of pores and throats is then generated with properties (radius, volume etc.) extracted from the original voxel representation. The cross-sectional shape of individual network elements (pores or throats) is a circle, square or triangle with the same shape factor, $G = A/P^2$, as the voxel representation, where A is the cross sectional area and P the perimeter length. Using square or triangular shaped network elements allows for the explicit modeling of wetting layers if non-wetting phase occupies the center of the element and wetting phase remains in the corners, Figure 2.

During primary oil flooding all elements are initially completely full of water, with displacement only occurring through piston-like displacement, where an oil-filled element can fill a neighboring water-filled element once the capillary entry pressure P_c is exceeded, given by the Young-Laplace equation. For a circular pore where we know the contact angle at which the interface hits the solid surface we can use the expression

$$P_c = \frac{2\sigma_{ow}\cos\theta_r}{r}, \tag{1}$$

where σ_{ow} is the oil-water interfacial tension, θ_r is the receding oil-water contact angle and r is the inscribed radius. The part of the rock in direct contact with oil may have its wettability altered following primary oil flooding, whereas the corners and elements still only containing water will remain strongly water-wet, Figure 2 (b). In addition to wettability alteration, contact angles are affected by the direction of flow. Due to surface roughness, advancing contact angles θ_a (increase in water saturation) are typically found to be significantly larger than receding contact angles θ_r (reduction in water saturation) [10]. With wettability alteration and water in corners the mechanisms by which water can displace oil become more complex [11]. The three main processes are piston-like displacement, pore body filling and snap-off. During forced water injection (negative capillary entry pressure) a layer of oil might become sandwiched between water in the corner and that in the center, Figure 2 (d). Stable oil layers can significantly increase recovery as it increases oil connectivity in much the same way that water layers influence primary oil flooding.

NETWORK MODIFICATION

When using pore-scale modeling to predict experimental data it is clearly important that the underlying network is representative of the rock. However, if the exact rock type has to be used for the network construction the application of predictive pore-scale modeling will be severely limited due to the complexity and cost of methods such as X-ray microtomography. In this section we will use the topological information of a reference Berea network [9] (relative pore locations and connection numbers) while tuning the properties of the individual network elements using capillary pressure and NMR data, enabling a wide range of experimental data from several types of porous media to be predicted. The reference network covers a rock volume of 3^3 mm^3, consisting of 12,349 pores and 26,146 throats. The connection numbers varies between 1 and 19, with an average of 4.19. The porosity of the network is 0.24 with an absolute permeability of 2.7 Darcy.

The main geometric property influencing multiphase flow through porous medium is the distribution of pore sizes – in terms of inscribed radii and volumes. From experimental capillary pressure during forced displacement it is possible to obtain an initial estimate of the throat size distribution by assuming the network to be a bundle of capillary tubes. Using this distribution to populate the properties of the network model will typically not result in the predicted capillary pressure to be close to the experimental values. This indicates the difficulty of predicting multiphase data – the capillary pressure and relative permeabilities are influenced by the spatial distribution of pores and throats and their connectivity, something that cannot be captured using a bundle of capillary tubes assumption. The distribution of throat sizes is subsequently modified iteratively until an adequate match is obtained against the experimental data, with individual network elements assigned inscribed radii from the target distribution while still preserving their rank order – that is the largest throat in the network is given the largest radius from the target distribution and so on. This should ensure that size correlations between individual elements and on larger scales are maintained.

Experimental capillary pressure is typically well described for uni-modal pore size distributions by the function

$$P_c = P_{ce}\left(\frac{1-S_{wc}}{S_w - S_{wc}}\right)^{\lambda}, \tag{2}$$

where P_{ce} is the entry capillary pressure and λ is a regression constant describing the pore space tortuosity. In Figure 3 (a) the capillary pressure for various values of λ has been matched, assuming a constant capillary entry pressure of 4,500 Pa for this set of curves. Other properties of the network are given Table 1. In order for the reference Berea network to have a similar entry pressure, all length scales were scaled by a factor of $\sqrt{K^{ref}/K^{net}}$ with a target permeability, K^{net}, of 1000 mD. The capillary pressure of the modified network was subsequently matched with a λ value of 0.54.

The effect on primary oil flooding relative permeability is shown in Figure 3 (b). Flow rate through an element (pore or throat) scales to the fourth power of inscribed radius [12]. Since the larger elements will be invaded first during forced oil flooding, an increasing λ, resulting in a widening of the throat size distribution, will result in a rapid decline of the oil relative permeability. Similarly, towards the end of primary oil flooding, the displacement of the smaller elements of the network will add little to the water relative permeability. However, the concave part of the oil relative permeability curve will often not be observed experimentally due to the high capillary pressures required.

In the network there is no direct relationship between the radius and volume of an element due to both properties being obtained directly from the original voxel representation. All the modified networks so far have thus had the same normalized pore volume distribution (scaled with respect to effective pore volume). Scaling individual pore volumes V by

$$V = \frac{V_0^a}{\overline{V}_0^{a-1}}, \tag{3}$$

where V_0 is the original pore volume, $\overline{V}_0$ is original median volume and a is a scaling factor, results in relatively little change in capillary pressure response, Figure 4. The effect on relative permeability is however much more pronounced, Figure 5 (a). Changes in the volume distribution only affect the saturation at a given capillary pressure, with no effect on the filling sequence or network conductance. However, in most cases one would expect there to be some relation between the throat radii and pore volumes. From Figure 5 (b) it is clear that during primary oil flooding the effect from changes in throat sizes is partly offset by the changes in volume distribution.

For realistic modeling of flow in porous media it is difficult to a priori determine the relation between throat radii and pore volumes without direct measurements using for example micro-CT technology. One possibility is to use NMR data to constrain the distribution of pore volumes. Assuming that the T_2 surface relaxation time for a pore is given by

$$\frac{1}{T_2} = \rho_2 \left(\frac{S}{V} \right)_{pore}, \tag{4}$$

where ρ_2 is the T_2 surface relaxivity (assumed to be 15 μm/s for this work) and S is the pore surface area, a T_2 distribution can be estimated. In Figure 6 the predicted T_2 distributions corresponding to Figure 5 (b) is shown.

TRENDS DURING WATER FLOODING

The wetting condition of the porous medium is of great importance in defining the flow characteristics during water flooding. Three broad classifications can be identified – strongly water-wet, strongly oil-wet or intermediate-wet. A combination of these wetting

conditions is also possible. We will refer to this latter condition as mixed-wet – most hydrocarbon bearing reservoirs are found to fall into this category [13].

In this section we will focus water-wet, mixed-wet and oil-wet systems. Water-wet advancing contact angles are distributed uniformly between 15 and 75 degrees and oil-wet advancing contact angles between 155 and 175 degrees. The wetting state of the network is measured using the Amott index [14], measuring the fraction of each phase that spontaneously imbibes. For the mixed-wet cases we set an Amott water index of 0.45 and an oil index of 0.30. This is achieved by assigning about 0.52 of the pore space (by volume) to be oil-wet. The oil-wet elements are distributed on the pore scale in spatially correlated patches [6] with a correlation length of about 7 pores. This wettability characterization scheme might occur in scenarios where clay minerals are important in determining what part of the pore space becomes oil wet [15] and is found to predict experimental data well. It is important to note that this is just one possible scenario for mixed-wetting. Distributing oil-wet elements based on pore size [16, 17] or changing the distribution of contact angles will influence both the shape of the relative permeability curve as well as the residual saturation [6, 17].

Relative permeability is strongly influenced by the pore space tortuosity in cases where a significant portion of the pore space is water-wet, Figure 7. In the strongly water-wet cases, residual oil saturation increases from 0.3 to 0.6 as the tortuosity exponent λ increases from 0.2 to 1.4. During spontaneous imbibition water will first enter the smallest elements, by piston-type displacement or by snap-off. Once filled by water, oil can no longer escape through that element, eventually resulting in trapped clusters of oil. A wider distribution of throat radii and pore volumes will result in increased dominance of throats filling by snap-off while the pores, containing most of the volume, become trapped. In the mixed-wet cases the residual oil saturation is varying between 0.07 and 0.20, due to the oil-wet elements maintaining pathways for the oil to escape. There is, however, a large impact on the relative permeability as the tortuosity increases. As snap-off fills water-wet throats, oil connectivity is quickly reduced, but without much change to the overall water saturation. During forced displacement, water will preferentially enter the larger elements, resulting in a rapid increase in saturation. Since snap-off is largely suppressed during forced displacement, there is less variation in the relative permeability for the strongly oil-wet case, with a behavior largely similar to primary oil flooding. Until a spanning cluster of elements containing bulk water exists across the network, water relative permeability will remain very low, less than 10^{-5}, due to water connectivity existing only through crevice water films.

The influence of varying the oil-wet fraction of the pore space, β, is shown in Figure 8. At low fractions no connected pathways of oil-wet elements can be created, resulting in those elements becoming trapped before any forced displacement can take place. Once the percolating threshold is reached, at a fraction of about 0.4, the residual oil saturation is significantly reduced. At high oil-wet fractions there is a significant amount of trapped

water during secondary oil flooding. This is the result of stable oil films preventing water in the bulk of the pore space to escape through the connected water films in the crevices.

PREDICTING EXPERIMENTAL DATA

To validate the model we need to compare against experimental results. We will first focus on water-wet experimental data where the pore-level wettability is fairly easily characterized. We will start with data from Berea sandstones, where we know we have an appropriate network, allowing us to validate the basic network model. Subsequently we will investigate flow in mixed-wet and oil-wet media. This poses a challenge since we have to modify our network while at the same time try to characterize the pore-level wetting state.

Water-Wet Berea Sandstone

Predicted relative permeability for primary oil flooding and water flooding are compared to steady-state experimental data by Oak [18] in Figure 9. During primary oil flooding the network is assumed to be strongly water-wet with a receding contact angle of 0 degrees. There are no other parameters to adjust, with all geometric network properties (connection numbers, radii, shape factors etc.) defined in the sandstone reconstruction process. While the network is still water-wet during water flooding the advancing contact angles will be larger, due to roughness of the surface and minor wettability alteration. The prediction shown in Figure 9 (b) was obtained with advancing contact angles uniformly distributed between 55 and 80 degrees. Small changes in the distribution of contact angles did not significantly affect the results, as long as the system remained water-wet. Additional fluid and rock parameters are given in Table 1.

Mixed-Wet Reservoir Sandstone

Capillary pressure data are usually available from centrifuge or mercury intrusion experiments. . For this example we will use mercury-air capillary pressures to modify the network and then predict relative permeability. Though only available for the primary flooding cycle, this data has the benefit of not being influenced by wettability characterization issues as the mercury-air contact angle is assumed fixed at 120 degrees with an interfacial tension of 0.48 N/m.

The capillary pressure response of the network model was matched to experimental data for a reservoir sandstone, with the mercury-air data rescaled to oil-brine properties, and the results are shown in Figure 10 (a). The experimental data was also matched using Eq. (2) with a λ of 0.37. Since no spontaneous displacement or NMR data were available, the normalized pore body volume distribution of the original Berea network was retained. A minimum pore throat radius of 1 μm was chosen to set connate water saturation in this case, resulting in $S_{wc} = 0.11$. The initial water saturation is adjusted such that S_{wc} in the network model is consistent with experimental data in both capillary pressure and relative permeability measurements.

Following aging the sandstone exhibited mixed-wet characteristics with an Amott water index of 0.55, indicating that about half the pore space had become oil-wet. No oil index was measured. Rock properties used in the relative permeability predictions, Figure 10 (b), are given in Table 1. Predictions of both the relative permeability and Amott water index, predicted value of 0.56, are in good agreement with the experimental values.

Oil-Wet Reservoir Sandstone

The final sandstone dataset had steady-state relative permeabilities measured on 2 core samples [6]. Since no mercury injection data were available, primary oil flooding centrifuge capillary pressure had to be used for the network modification process, Figure 11 (a). Following wettability alteration the core exhibited mainly oil-wet characteristics with Amott water and oil indices of 0.00 and 0.14. The comparison between experimental and predicted relative permeability is shown in Figure 11 (b). The low residual oil saturation is also an indication of an oil-wet system, a result of oil being able to escape through layers. Water relative permeability will remain very low, less than 10^{-5}, until a spanning cluster of elements containing bulk water exists across the network. The predictions were made with S_{wi} = 0.02 and the predicted Amott indices of 0.00 and 0.15 for water and oil respectively are in good agreement with experimental values.

CONCLUSIONS

Using a geologically realistic network initially developed to represent Berea sandstone we predicted flow properties for several experimental datasets. This suggests that a realistic network topology combined with network properties tuned to experimental data such as mercury injection capillary pressure and NMR T_2 distribution can be used to predict single and multiphase properties for a wide range of porous media. For this work we have only used a single network constructed from Berea sandstone. To improve confidence in predictions from a wider range of rocks, including carbonates, it would be preferable to have a library of networks representing different rock types. The network that most closely matches the geological structure of the sample of interest would then be chosen for modeling studies.

REFERENCES

1. Bakke, S. and P.E. Øren, "3-D pore-scale modelling of sandstones and flow simulations in the pore networks," *SPE Journal*, (1997) **2**, 2, p. 136-149.
2. Adler, P.M. and J.F. Thovert, "Real porous media: Local geometry and macroscopic properties," *Applied Mechanics Reviews*, (1998) **51**, 9, p. 537-585.
3. Silin, D.B. and T.W. Patzek, "Robust Determination of the Pore Space Morphology in Sedimentary Rocks," 2003 SPE Annual Technical Conference and Exhibition, SPE 84296, 2003, Denver.
4. Øren, P.E., S. Bakke, and O.J. Arntzen, "Extending predictive capabilities to network models," *SPE Journal*, (1998) **3**, 4, p. 324-336.
5. Blunt, M.J., et al., "Detailed physics, predictive capabilities and macroscopic consequences for pore-network models of multiphase flow," *Advances in Water Resources*, (2002) **25**, 8-12, p. 1069-1089.

6. Valvatne, P.H. and M.J. Blunt, "Predictive Pore-Scale Network Modeling," 2003 SPE Annual Technical Conference and Exhibition, SPE 84550, 2003, Denver.
7. Patzek, T.W., "Verification of a complete pore network simulator of drainage and imbibition," *SPE Journal*, (2001) **6**, 2, p. 144-156.
8. Blunt, M.J., "Physically-based network modeling of multiphase flow in intermediate-wet porous media," *Journal of Petroleum Science and Engineering*, (1998) **20**, 3-4, p. 117-125.
9. Lerdahl, T.R., P.E. Øren, and S. Bakke, "A Predictive Network Model for Three-Phase Flow in Porous Media," SPE/DOE Symposium on Improved Oil Recovery, SPE 59311, 2000, Tulsa.
10. Morrow, N.R., "Effects of surface roughness on contact angle with special reference to petroleum recovery," *Journal of Canadian Petroleum Technology*, (1975) **14**, 4, p. 42-53.
11. Lenormand, R., C. Zarcone, and A. Sarr, "Mechanisms of the Displacement of One Fluid by Another in a Network of Capillary Ducts," *Journal of Fluid Mechanics*, (1983) **135**, OCT, p. 337-353.
12. Patzek, T.W. and D.B. Silin, "Shape factor and hydraulic conductance in noncircular capillaries I. One-phase creeping flow," *Journal of Colloid and Interface Science*, (2001) **236**, 2, p. 295-304.
13. Anderson, W.G., "Wettability Literature Survey - Part 1: Rock-Oil-Brine Interactions and the Effects of Core Handling on Wettability," *Journal of Petroleum Technology*, (1986) **38**, 11, p. 1125-1144.
14. Anderson, W.G., "Wettability Literature Survey - Part 2: Wettability Measurement," *Journal of Petroleum Technology*, (1986) **38**, 12, p. 1246-1262.
15. Durand, C. and E. Rosenberg, "Fluid distribution in kaolinite- or illite-bearing cores: cryo-SEM observations versus bulk measurements," *Journal of Petroleum Science and Engineering*, (1998) **19**, 1-2, p. 65-72.
16. Kovscek, A.R., H. Wong, and C.J. Radke, "A Pore-Level Scenario for the Development of Mixed Wettability in Oil-Reservoirs," *AIChE Journal*, (1993) **39**, 6, p. 1072-1085.
17. Man, H.N. and X.D. Jing, "Network modelling of mixed-wettability on electrical resistivity, capillary pressure and wettability indices," *Journal of Petroleum Science and Engineering*, (2002) **33**, 1-3, p. 101-122.
18. Oak, M.J., "Three-phase relative permeability of water-wet Berea," SPE/DOE Seventh Symposium on Enhanced Oil Recovery, SPE 20183, 1990, Tulsa.

Table 1. Fluid and rock properties used in network model.

Property	Initial net. properties	Water-wet Berea sst.	Mixed-wet sandstone	Oil-wet sandstone
Porosity	0.25	0.24	0.27	0.15
Permeability, K (mD)	–	2668	814	2302
Capillary entry pressure, P_{ce} (kPa)	–	2480	5300	3170
Connate water saturation, S_{wc}	0.20	0.24	0.11	0.12
Lambda exponent, λ	–	0.54	0.37	0.60
Water-wet advancing contact angles, θ_a (deg)	15-75	55-80	0-75	10-40
Oil-wet advancing contact angles, θ_a (deg)	155-175	–	155-180	96-173
Oil-wet fraction by pore volume, β	–	0.00	0.43	1.00

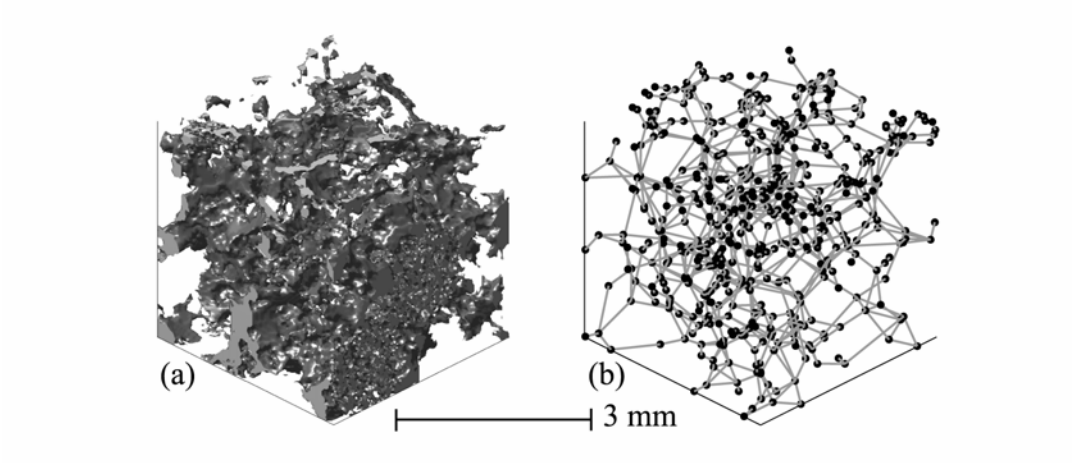

Figure 1. (a) Three-dimensional image of a sandstone along with (b) a topologically equivalent network representation [4].

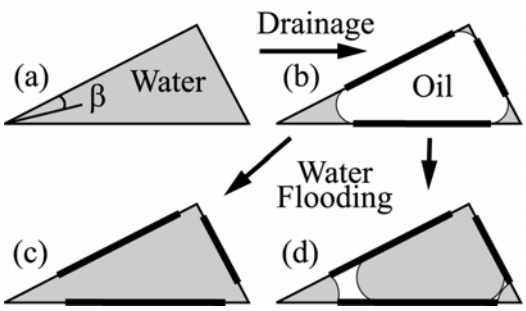

Figure 2. Possible fluid configurations. (a) Initially the element is water-filled and strongly water-wet. (b) Following primary oil flooding the part of the element in contact with oil will alter its wettability. (c) During water flooding the element might again become completely water-filled. (d) If wettability alteration was large enough, oil might become sandwiched as a layer between water in the corner and the center.

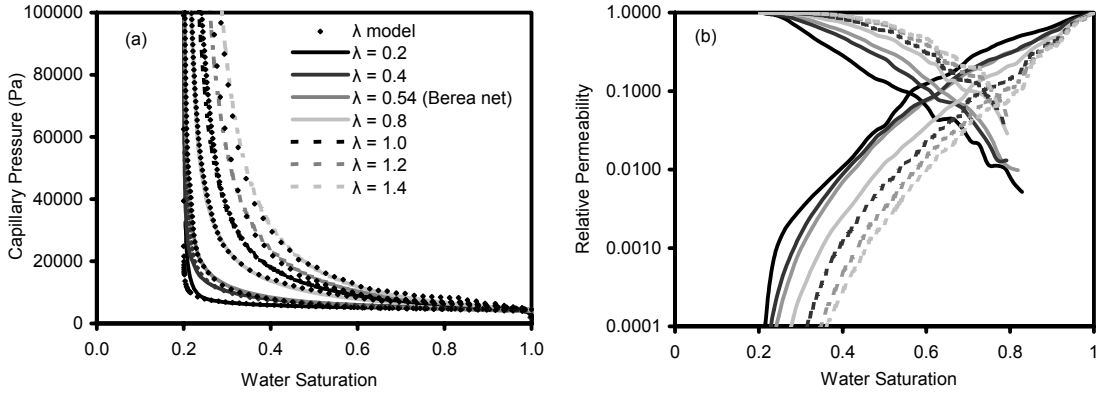

Figure 3. (a) The capillary pressure for different values of λ is matched by modifying the throat size distribution of network. The capillary pressure of the reference Berea network (scaled to a 1000mD) is matched with a λ value of 0.54. (b) Effect on primary oil flooding relative permeability from variations in throat size distribution.

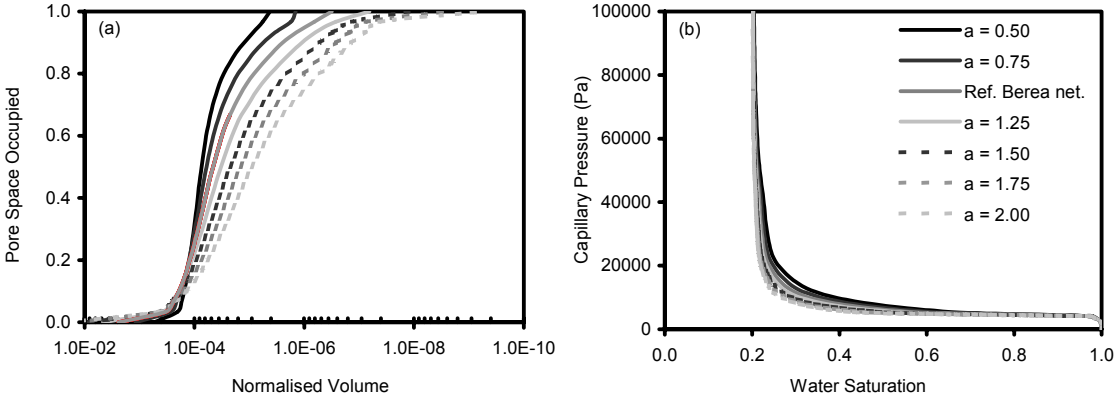

Figure 4. The effect from scaling individual pore volumes (a) is relatively minor on the capillary pressure response (b).

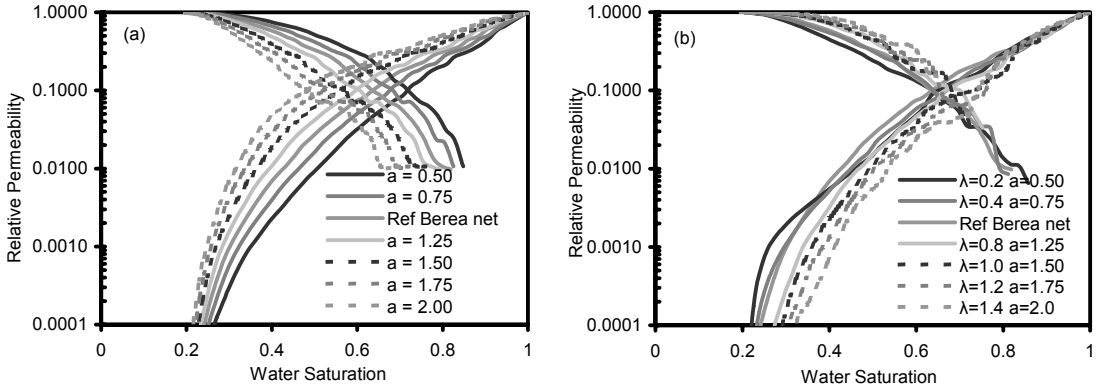

Figure 5. Effect on primary oil flooding relative permeability from variations in pore volume distribution (a) and by combining changes in both throat sizes and pore volumes (b).

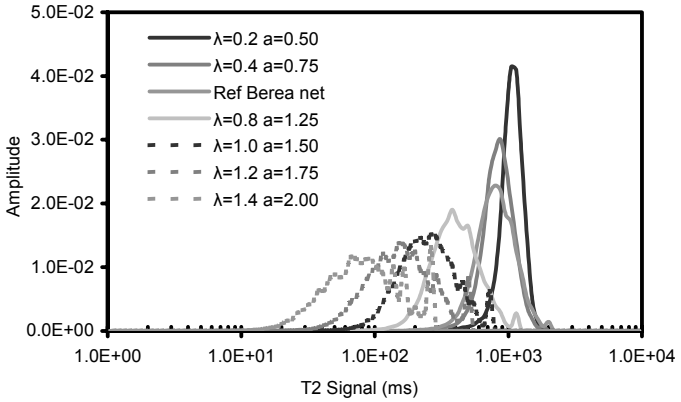

Figure 6. Estimated T_2 distribution can be used to constrain the pore volume distribution used in the network model.

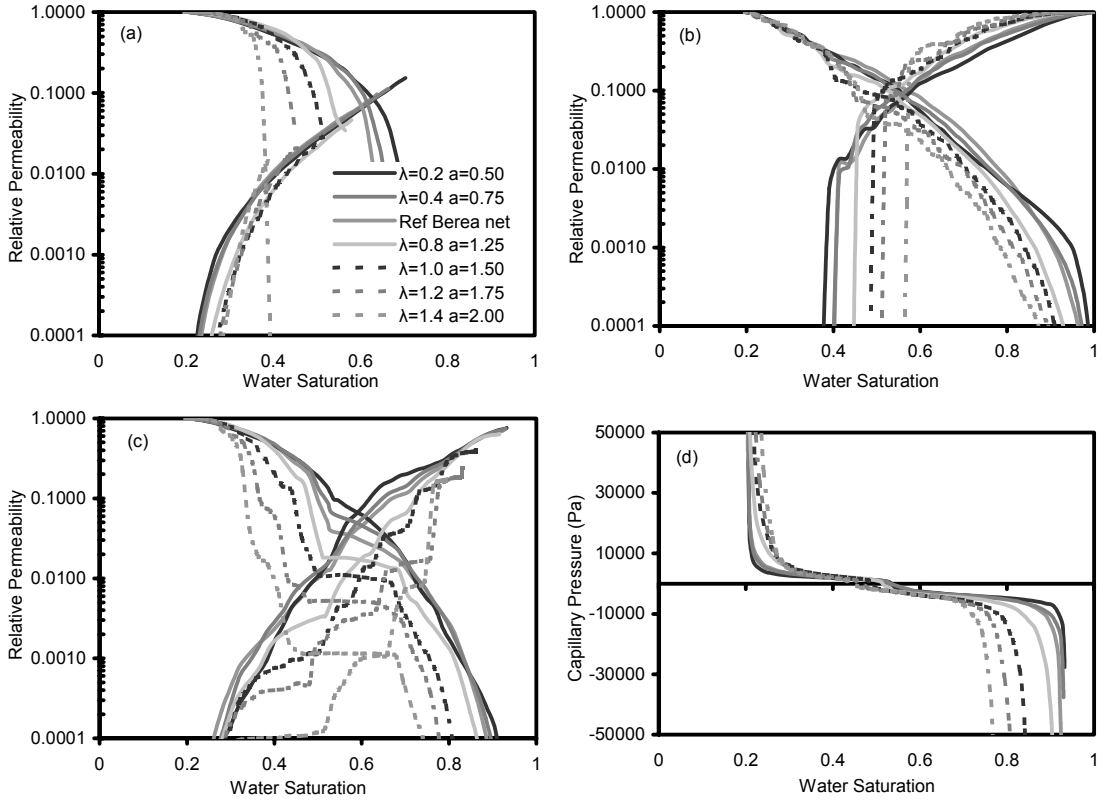

Figure 7. Influence of wettability and geometric properties on water flooding relative permeability. (a) For water-wet conditions increasing pore space tortuosity will result in higher residual oil saturation. (b) In oil-wet conditions the displacement is forced, resulting in similar behavior to primary oil flooding. Water relative permeability will stay very low, less than 10^{-5}, until a spanning cluster of bulk water filled elements exists across the network. (c) There is a strong influence of geometric properties in mixed wet conditions. (d) About half the pore was assigned oil-wet characteristics for mixed-wet conditions, as evident from the capillary pressure.

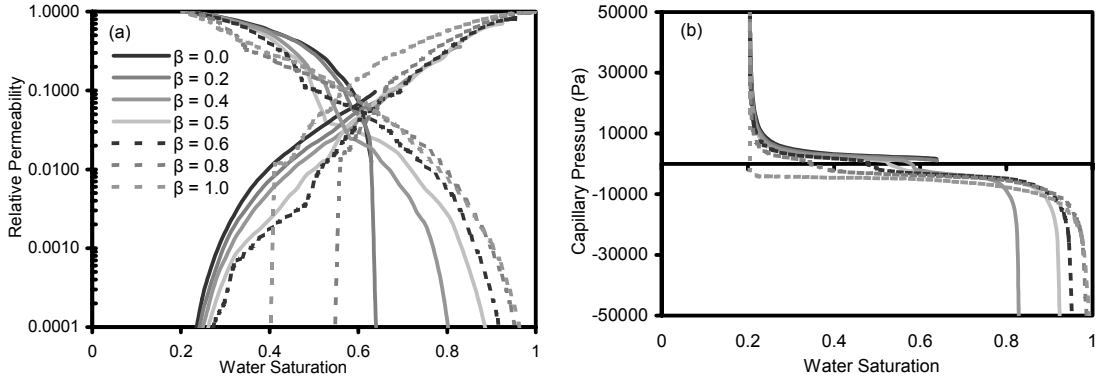

Figure 8. Influence of oil-wet fraction, β, on relative permeability (b) and capillary pressure (c). Once the percolating threshold of oil-wet elements has been reached, residual oil saturation is significantly reduced.

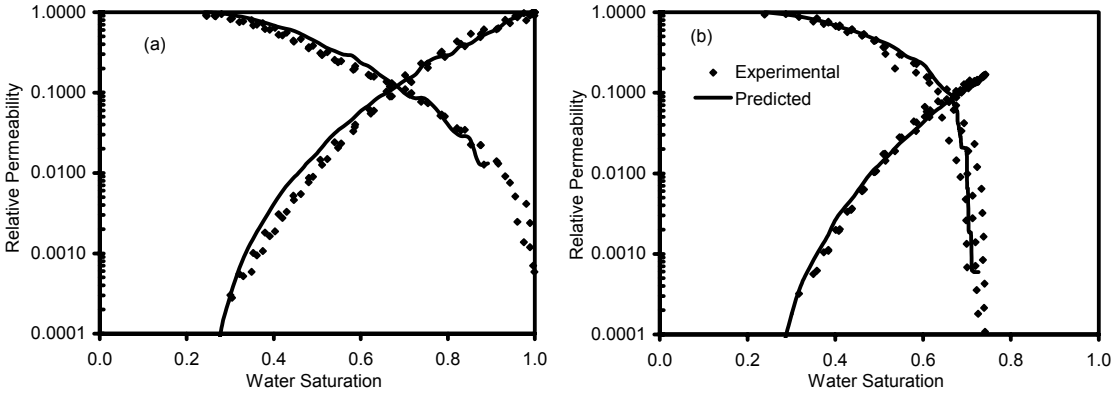

Figure 9. Predicted primary oil flooding (a) and secondary water flooding (b) relative permeability for water-wet Berea sandstone (lines) compared to experimental data by Oak [18] (squares).

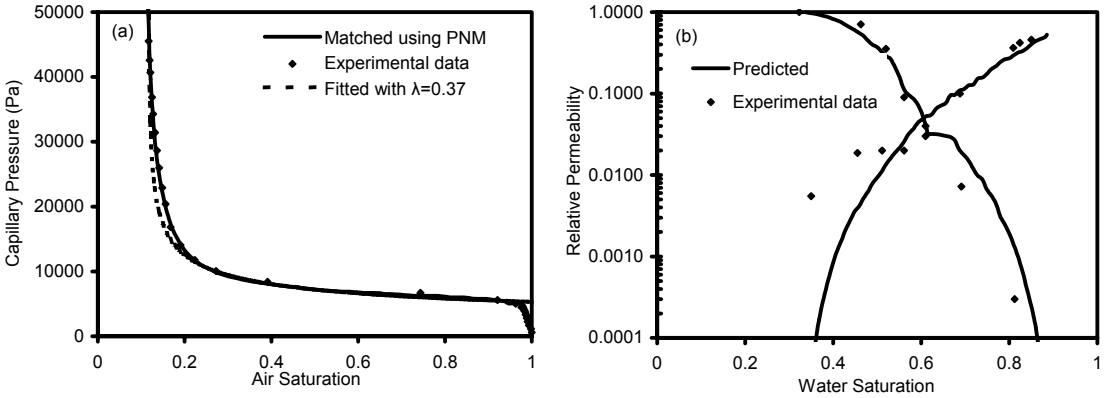

Figure 10. Predicting mixed-wet experimental data. (a) Comparison between experimental, pore network model (PNM) matched and λ fitted mercury-air capillary pressure (rescaled to oil-brine properties). (b) Comparison between experimental and predicted relative permeability.

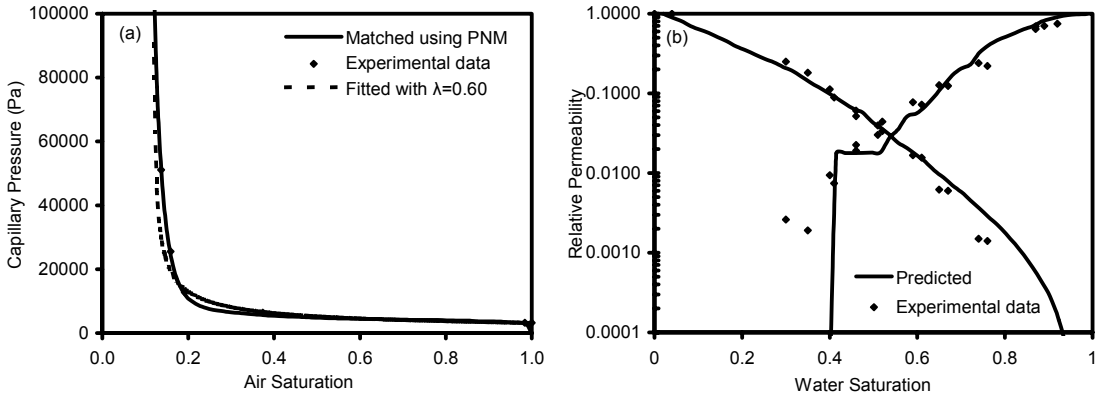

Figure 11. Comparison between predicted and experimental properties for oil-wet reservoir sandstone. (a) Centrifuge primary oil flooding capillary pressures were used to modify the network. (b) Predicted water flooding relative permeabilities are compared to experimental steady-state data. Low residual oil saturation is a good indication oil-wet characteristics.